



Original scientific paper

## Functionalization of FeCoNiCu medium entropy alloy via nitridation and anodic oxidation for enhanced oxygen evolution and glycerol oxidation

Luka Suhadolnik<sup>1,✉</sup>, Milutin Smiljanić<sup>1,✉</sup>, Marjan Bele<sup>1</sup>, Mejrema Nuhanović<sup>1</sup>, Matjaž Finšgar<sup>2</sup>, Nik Maselj<sup>1</sup>, Daniela Neumüller<sup>3</sup>, Lidija D. Rafailović<sup>3</sup> and Nejc Hodnik<sup>1,4,✉</sup>

<sup>1</sup>Department of Materials Chemistry, National Institute of Chemistry, Hajdrihova 19, SI-1000 Ljubljana, Slovenia

<sup>2</sup>Faculty of Chemistry and Chemical Engineering, University of Maribor, Smetanova 17, 2000 Maribor, Slovenia

<sup>3</sup>Department of Materials Science, Chair of Materials Physics, University of Leoben, Jahnstrasse 12, 8700, Leoben, Austria

<sup>4</sup>Institute of Metals and Technology, Ljubljana 1000, Slovenia

Corresponding authors: ✉ [luka.suhadolnik@ki.si](mailto:luka.suhadolnik@ki.si); ✉ [milutin.smiljanic@ki.si](mailto:milutin.smiljanic@ki.si); ✉ [nejc.hodnik@ki.si](mailto:nejc.hodnik@ki.si)

Received: December 27, 2024; Accepted: February 5, 2025; Published: February 18, 2025

### Abstract

Medium entropy alloys (MEAs) have emerged as a promising class of materials for electrocatalysis due to their tunable properties and exceptional catalytic performance. This study successfully functionalized a bulk FeCoNiCu alloy using a combined anodic oxidation (AO) and nitridation (NT) approach to produce a highly porous, thin-film catalyst. The hierarchical structure formed during the surface treatments enhances the material's specific surface area and alters the oxidation states of the constituent metals, creating abundant active sites. The electrocatalytic performance of the modified bulk FeCoNiCu electrode was evaluated for both the oxygen evolution reaction (OER) and glycerol oxidation reaction (GOR) in an alkaline electrolyte. Remarkably, the AO-NT-treated catalyst exhibited superior activity for OER, surpassing commercial IrO<sub>x</sub> benchmarks with lower overpotential requirements. For GOR, the FeCoNiCu electrode demonstrated excellent performance by significantly reducing energy input compared to OER, highlighting its potential as a dual-purpose catalyst for alkaline water splitting. Post-reaction product analysis via NMR confirmed the formation of value-added chemicals, with formic acid identified as the main product. These results underline the feasibility of surface-modified MEAs for sustainable energy and chemical production applications, offering a cost-effective alternative to noble metal-based catalysts.

**Keywords**

Medium entropy alloy, surface modification, electrocatalysis, oxygen evolution reaction, glycerol oxidation

---

**Introduction**

Medium entropy alloys (MEAs), a subset of compositionally complex materials (CCMs), have emerged as an exciting new class of materials due to their unique microstructures and tunable properties [1]. Unlike conventional alloys, MEAs typically combine three to five elements in near-equiatom proportions, resulting in complex atomic arrangements that provide an exceptional synergy of mechanical, thermal, chemical, and electronic properties [2,3]. The inherent flexibility in elemental composition allows MEAs to exhibit unique features such as high hardness, excellent corrosion resistance, remarkable thermal stability, and unique catalytic properties, making them promising candidates for various applications [4-6]. However, the general shortcoming of CCMs is that they usually come with low specific surface area, which impedes their practical applications in electrocatalysis. To address this, further adjustments of the MEAs' properties can be achieved through surface modifications such as anodic oxidation (AO) and nitridation (NT). AO is known for its relative simplicity and the possibility to create highly porous structures with enlarged surface area, while NT introduces nitrides and oxynitrides into the material, which can significantly improve electronic properties, hardness, wear resistance, and thermal stability. When applied in tandem, these two surface treatments can synergistically boost the overall properties of MEAs, unlocking new possibilities for their applications [7].

Electrocatalysis is one of the fields where the application of CCMs has become particularly attractive due to the constant pursuit of improved catalytic materials [8]. The concept of green hydrogen energy is particularly attractive, and the development of active, durable, and affordable electrocatalysts for electrochemical water splitting is crucial [9]. The bottleneck in water electrolysis is the anodic oxygen evolution reaction (OER), which is kinetically sluggish and takes place under harsh conditions (elevated potentials, extreme pH, and high temperatures), therefore demanding the usage of precious metals catalysts such as Ir and Ru (and their oxides) [10]. To overcome these issues, two strategies can be applied: (i) to develop non-noble catalysts for OER able to compete with Ir- and Ru-based benchmarks; (ii) to substitute OER with some other less energy-demanding anodic reaction, such as glycerol oxidation reaction (GOR) [11,12]. Both strategies can be covered by exact and guided synthesis and modifications of CCMs to yield unique active sites thanks to the fine-tuning of the composition and morphology of these catalysts. Our recent study showcased the potential of the combination of NT-AO applied to FeCoNiCuZn alloy to produce a tuned structure with exceptional electrocatalytic activity for water oxidation in alkaline electrolytes [7]. While NT only slightly improved the activity of starting FeCoNiCuZn alloy, subsequent AO boosted its performance even beyond commercial IrO<sub>x</sub> reference catalysts and placed it among the best-performing non-noble catalysts for OER in the literature. This was explained by the significant increase in the catalysts' surface area and changes in the composition of the CCM induced by NT-AO. Specifically, NT-AO treatment removed Cu and Zn, resulting in a hierarchically connected pore structure, where larger pores are interlinked with smaller ones formed due to fluorides in the AO electrolyte, while also altering the oxidation states of the constituent metals. In the case of GOR, noble metal catalysts such as Pt, Pd, and Au are highly effective, offering excellent catalytic properties and stability [13]. Nickel-based materials offer cost-effective alternatives with promising GOR activity, especially when paired with cobalt, which further boosts catalytic performance [14,15]. Combining non-noble and noble metals into multi-metallic and alloy catalysts, such as bimetallic

PtAg [16] or Ni<sub>80</sub>Pd<sub>20</sub> [17], can also enhance catalytic efficiency through synergistic effects. Although MEAs and CCMs are generally gaining increasing attention in electrocatalysis, their application in GOR remains underexplored [18]. The vast potential for incorporating various elements into CCMs offers a broad field for experimentation, with many influences on catalytic performance yet to be understood. Future research should focus on testing a wider range of CCMs for reactions such as GOR to fully exploit their potential and enhance the efficiency and selectivity of these processes. For instance, HEA - CoNiCuMnMo nanoparticles synthesized on carbon cloth have shown high efficiency in glycerol oxidation reaction, with molybdenum sites coordinated by manganese, molybdenum, and nickel identified as key catalytic centres [19]. Another study reported Pt-decorated FeCoNiCuMn HEA nanocatalysts with a superior GOR performance compared to Pt/C, which was ascribed to the composition of HEA, providing better CO poisoning features on Pt-sites [20]. These studies show a high potential for HEA in GOR catalysis and underscore the need for further exploration in this domain [19].

In this study, a highly porous, thin film electrocatalyst was synthesized by surface modification of the FeCoNiCu bulk electrode and tested for both GOR and OER in an alkaline electrolyte. The starting FeCoNiCu CCM was modified using the AO-NT procedure, and the obtained thin film exhibited promising catalytic properties for both OER and GOR. The catalyst was thoroughly analysed to confirm its composition, structure, and electrocatalytic performance, providing important insights for future optimization and practical applications. While further studies are necessary, the results demonstrate that the FeCoNiCu bulk alloy electrode, modified by the NT-AO approach, represents a very promising concept for developing highly active anodes for alkaline water electrolysis.

## Experimental Section

### *Catalyst preparation*

The catalyst was prepared following conditions reported by Suhadolnik *et al.* [7]. Briefly, a compositionally complex FeCoNiCu alloy was produced by arc-melting high-purity elements in a Ti-getter Ar atmosphere, followed by multiple heating and cooling cycles for homogeneity. The alloy was nitridized at 700 °C for 30 minutes in ammonia flow, then anodized at 50 V for 5 minutes in a custom electrochemical cell using the freshly prepared electrolyte.

### *Catalyst characterization techniques*

SEM and SEM-EDS analysis: The surface morphology of the catalyst was examined under the conditions previously reported by Suhadolnik *et al.* [21].

XRD analysis: The catalyst was characterized using X-ray diffraction as described by Suhadolnik *et al.* [7]. Phase identification was carried out with the X'Pert HighScore Plus software, utilizing the ICDD PDF-4+ 2024 database [21].

XPS analysis: The surface composition of the compositionally complex sample was analysed using X-ray photoelectron spectroscopy (XPS) using a Supra+ instrument equipped with an Al K<sub>α</sub> excitation source. Spectra were acquired and processed using ESCAPE 1.5 software. XPS measurements were performed at a 90° take-off angle using 160 eV pass energy (survey spectrum). The binding energy ( $E_B$ ) scale was corrected using the C-C/C-H peak in the C 1s spectrum, which is located at 284.8 eV. The size of the XPS analysis spot was 300 by 700 μm.

ToF-SIMS analysis: Depth profiling was performed using a ToF-SIMS M6 instrument (IONTOF, Münster, Germany) equipped with a Bi liquid metal ion gun and a Cs<sup>+</sup> sputtering source. The primary Bi<sup>+</sup> ion beam was operated at 30 keV (1.0 pA), while sputtering was performed using 2 keV Cs<sup>+</sup>

(205 nA). Sputtering was performed over an area of 500 by 500  $\mu\text{m}$ , while the analysis was performed in the middle of the sputter crater on an area of 300 by 300  $\mu\text{m}$ . Spectra were acquired and processed using SurfaceLab 7.3 software (IONTOF, Münster, Germany).

NMR experiments were performed on a Bruker AVANCE NEO 600 MHz spectrometer equipped with a 5 mm BBFO probe. Spectra was measured in deuterated water ( $\text{D}_2\text{O}$ , Sigma Aldrich).  $^1\text{H}$  NMR spectra were referenced on 3-(Trimethylsilyl) propionic-2,2,3,3- $\text{d}_4$  acid sodium salt (TMSPA) ( $\delta = 0.00$  ppm) and water present in the sample ( $\delta = 4.79$  ppm). The samples were prepared by sampling 100  $\mu\text{L}$  of the electrolyte after the electrolysis and adding 500  $\mu\text{L}$  of  $\text{D}_2\text{O}$ .

**Electrochemical analysis:** Electrochemical measurements were performed for both OER and GOR at ambient temperature in a single-compartment electrochemical cell with a three-electrode setup. The prepared catalyst was mounted in a custom-made Teflon holder, identical to the one used during anodization, and served as the working electrode. A HydroFlex reversible hydrogen electrode (RHE, Gaskatel GmbH) was used as the reference electrode, while a glassy carbon rod functioned as the counter electrode. A potentiostat (SP-300, Biologic) was used to control the potential. All voltammetric experiments included compensation (85 %) for the ohmic drop determined via electrochemical impedance spectroscopy (EIS) at high frequencies. A double-layer capacitance ( $C_{\text{dl}}$ ) approach was used to assess the electrochemical surface area of our catalyst, as described elsewhere [7]. Briefly, cyclic voltammetry (CV) was applied at different scan rates (20, 50, 100, 200, and 300  $\text{mV s}^{-1}$ ) in the potential range between 0.25 and 0.35  $V_{\text{RHE}}$ . Using linear dependence between  $\Delta j = j_a - j_c$  at  $E = 0.3 V_{\text{RHE}}$  and scan rate, the  $C_{\text{dl}}$  value was extracted. Linear sweep voltammetry (LSV) was performed in 1 M KOH for OER and in 1 M KOH with 0.1 M glycerol for GOR, over a potential range of 1.2 to 1.6 V vs. RHE (scan rate of 2  $\text{mV s}^{-1}$ ). Chronoamperometric (CA) measurements for GOR were conducted at various potentials in 1 M KOH containing 0.1 M glycerol. For OER activity comparison, a benchmark  $\text{IrO}_x$  catalyst was used (Premion, Alfa Aesar). The powdered catalyst was mixed with Milli-Q water (1 mg / 1 ml ratio) to form the uniform catalyst ink, which was then drop-casted (20  $\mu\text{L}$ ) onto glassy carbon (5 mm in diameter) rotating disk (RDE) resulting in catalyst loading of 102.04  $\mu\text{g cm}^{-2}$ . After drying,  $\text{IrO}_2$  films were covered with 5  $\mu\text{L}$  of Nafion:isopropanol mixture (volumetric ratio 1/50) to ensure adhesion. The electrochemical procedure included 20 cycles at a scan rate of 50  $\text{mV s}^{-1}$ , ranging from 0.05 to 1.45 V, followed by an activity assessment through linear sweep voltammetry (LSV) recorded from 1.2 to 1.6 V at 2  $\text{mV s}^{-1}$ . Both the activation and activity measurements were conducted in an argon-saturated electrolyte.

## Results and discussion

### *Morphology, composition, and structure of the compositionally complex catalyst*

The surface morphology of the catalyst was characterized using SEM (Figure 1a). The SEM micrographs, taken at various magnifications, reveal that the film is highly porous with a large surface area, exhibiting a hierarchical pore structure. The presence of both larger macropores and smaller mesopores is crucial for enhancing the exposure of active sites, which, through improved mass transport, enhances the adsorption-desorption dynamics of reactants and products [22]. This hierarchical porosity provides sufficient accessibility for larger molecules, while the high surface area of the mesopores supports effective catalytic reactions by increasing the number of accessible active sites. Moreover, the interconnected nature of the porous network may aid in the diffusion of reactants and the removal of products, reducing diffusion limitations and enhancing overall catalytic performance [23].

The XRD pattern of the catalyst is presented in Figure 1b. The diffractogram shows only peaks corresponding to the underlying FeCoNiCu alloy substrate, indicating that the highly oxidized porous film formed on top lacks sufficient crystallinity to generate distinct diffraction peaks. Due to the complexity of this multi-component alloy system and the absence of comprehensive reference cards in the XRD database for such complex materials, it is challenging to definitively assign specific peaks to individual phases. However, based on the composition determined by SEM-EDS and XPS analyses (as shown in Table 1), we can infer the presence of a single phase in the film. The amorphous nature of the oxidized film results from the synthesis conditions, which can lead to a disordered structure without sufficient crystallinity, *i.e.* a common characteristic of highly porous materials [24].

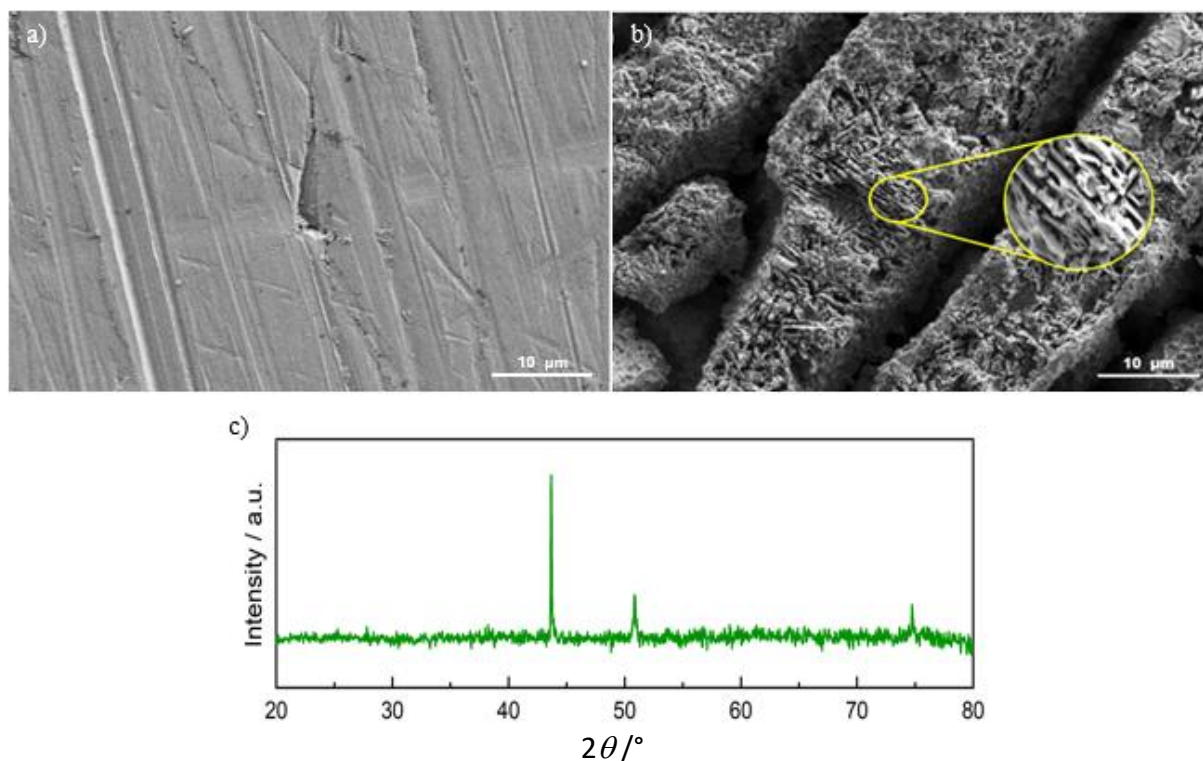


**Figure 1.** SEM micrographs showing: a) the initial alloy used for catalyst preparation, and b) the catalyst prepared with nitridation and anodization of the alloy shown at two magnifications. Inset circle diameter is 7  $\mu\text{m}$ . c) XRD diffractogram of the catalyst showing peaks related to the compositionally complex alloy

The XPS analysis confirmed the presence of Fe, Co, and Ni on the surface, while Cu was not detected (XPS survey spectrum in Figure 2). This indicates that Cu is either not present in the top few nanometres, *i.e.* the depth analysed by the XPS technique, or its concentration is below the detection limit of the XPS technique. However, as explained below, Cu was detected using ToF-SIMS, as this analytical technique has a significantly lower detection limit than XPS. The XPS survey spectrum shows intense Fe, Co, and Ni peaks with several XPS-induced LMM Auger peaks. However, the Fe 2p and Co 2p peaks overlap with other XPS-induced Auger peaks (Figure 2), a well-documented challenge in XPS analysis of alloy systems containing these elements. The intense O 1s peak indicates significant surface oxidation, while the presence of the C 1s peak indicates surface contamination, likely from adventitious carbonaceous species adsorbed from the environment after sample preparation during sample transfer to the XPS spectrometer.

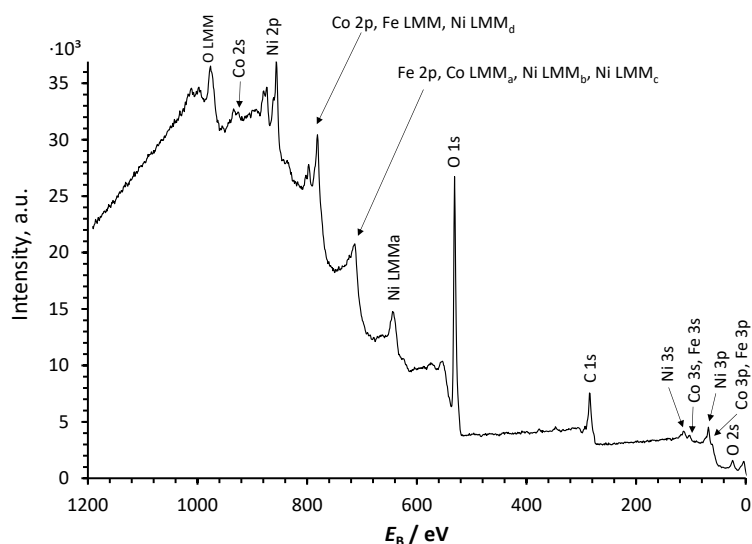


**Figure 2.** The XPS survey spectrum of the sample showing signals for Fe-, Co-, Ni-, C-, and O-containing species. The XPS surface analysis was performed after the electrocatalytic glycerol oxidation tests

Figure 3 presents the negative ion 3D ToF-SIMS images of the catalyst surface. In ToF-SIMS analysis, the  $M^-$  signal for a given element can originate from its metallic form (M), oxide ( $MO^-$ ), and/or hydroxide ( $MOH^-$ ). The  $MO^-$  signal primarily reflects metal oxides but can also include contributions from metal hydroxides. Similarly, the  $MOH^-$  signal primarily indicates metal hydroxides, although metal oxides can also contribute to this signal (by attaching very mobile hydrogen). The ToF-SIMS images show that Fe, Co, and Ni oxides/hydroxides dominate the catalyst surface (represented by the  $MO^-$  and  $MOH^-$  signals). In contrast, Cu oxides and hydroxides are detected at lower intensity. This distribution suggests that anodic oxidation primarily facilitates the formation of Fe, Co, and Ni oxides/hydroxides while Cu either dissolves, migrates, or forms sub-surface layers during the treatment.

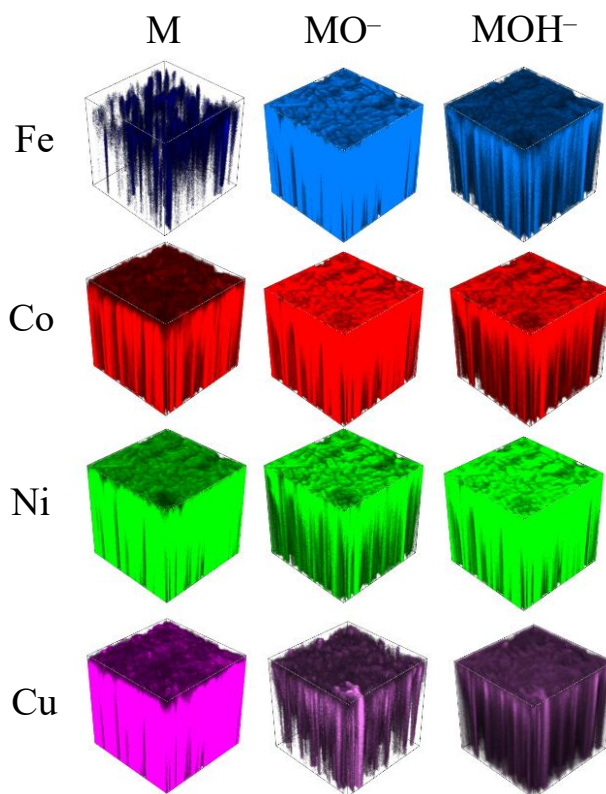


**Figure 3.** 3D ToF-SIMS images showing  $M^-$  ( $M = Ni, Fe, Ni$  or  $Co$ ), and the corresponding signal for  $MO^-$  and  $MOH^-$ . The analysis was performed after the electrocatalytic glycerol oxidation tests

Another explanation for the lower Cu presence could be selective leaching during anodic oxidation, leading to Cu depletion from the outermost layer. This effect aligns with the known behaviour of Cu under oxidative conditions, where more noble elements like Fe, Co, and Ni tend to stabilize on the surface. The transformation from metallic states to oxides and hydroxides reflects the anticipated outcome of anodic oxidation, which alters surface chemistry and enhances porosity and surface area, contributing to improved catalytic activity.

SEM-EDS analysis shows that the catalyst film is primarily composed of oxygen, iron, cobalt, and nickel, with Ni being the most abundant metal (Table 1). The EDS mapping analysis (Supplementary material, Figure S1) reveals a uniform elemental distribution. The significant presence of Ni, along with Fe and Co, suggests the formation of mixed metal oxides, which are known to enhance the catalytic activity of oxygen evolution reaction due to the availability of numerous Ni- and Co-based active sites and multiple oxidation states [25]. Copper is detected only in trace amounts, likely because it was removed during the anodic oxidation process, which, more importantly, also contributed to the increased porosity of the film.

**Table 1.** The chemical composition in of the compositionally complex catalyst was determined with SEM-EDS. Analysis was performed after the electrocatalytic glycerol oxidation tests.

Analysis	Content, at.%				
	Fe	Co	Ni	Cu	O
EDS	13.0	13.1	19.1	1.3	51.5

#### *Electrocatalytic glycerol oxidation performance*

The electrocatalytic performance of FeCoNiCu catalyst was determined in 1 M KOH (Titripur, Merck) in the absence and the presence of 0.1 M glycerol (Figure 3a). The electrocatalytic performance of FeCoNiCu catalyst was determined first for OER in 1 M KOH and compared to the IrO<sub>x</sub> benchmark, as shown in Figure 3. Besides a clear advantage in terms of cost, the treated FeCoNiCu catalyst is also more active than IrO<sub>x</sub> as it needs 54 mV less overvoltage to reach a current density of 10 mA cm<sup>-2</sup>. This comparison exemplifies the applicability of NT-AO-treated CCMs as OER catalysts. Furthermore, the same catalyst was tested for GOR, as shown in Figure 4. At the current density of 50 mA cm<sup>-2</sup>, the voltage difference between GOR and OER is 140 mV, which shows a significant decrease in the energy input needed to drive glycerol-assisted water splitting. A comparison of hereby developed material with recent literature data is given in Table S1. The determined C<sub>dl</sub> value for NT-AO-Treated FeCoNiCu catalyst was equal to 1.0 mF cm<sup>-2</sup> (see Figure S2), which is significantly lower compared to other literature reports on similar catalysts. This could indicate that despite necessitating a higher potential to reach the current density of 10 mA cm<sup>-2</sup>, the active sites present in NT-AO-treated FeCoNiCu have high specific activity. Therefore, by increasing the number of exposed active sites, the performance of the FeCoNiCu catalyst can be further boosted.

Product profiling during GOR was conducted using chronoamperometry at different potential values, as shown in Figure 4b. Based on the polarization curves in Figure 4a, it can be proposed that OER occurs at a negligible extent compared to GOR at the potentials used for chronoamperometric tests, as the significant OER currents are measured only at potentials above 1.5 V<sub>RHE</sub>. Except at the potential of 1.35 V<sub>RHE</sub>, the measured current densities show that significant glycerol oxidation takes place at the FeCoNiCu catalyst. The main products during glycerol oxidation experiments are expected to be liquid, and NMR was used to analyze the product distribution.

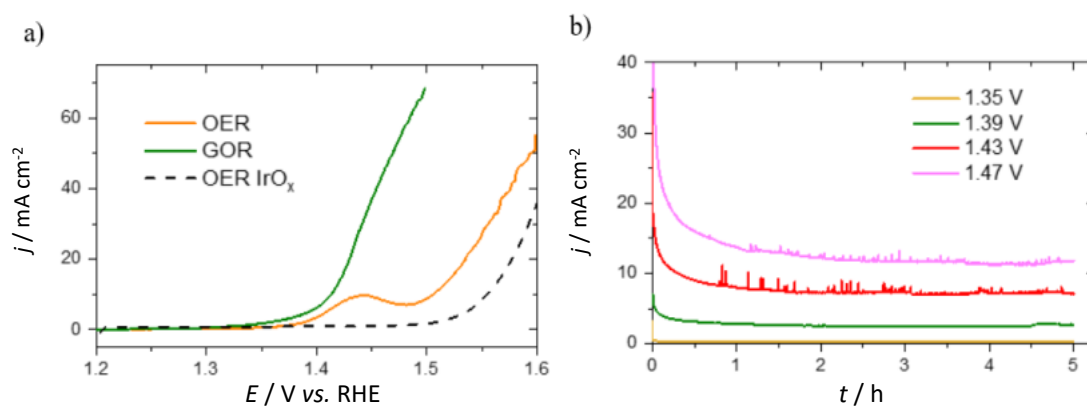


**Figure 4.** a) LSV polarization curves in 1 M KOH and 1 M KOH with 0.1 M glycerol. b) Chronoamperometric glycerol oxidation at varied potentials in 1 M KOH solution containing 0.1 M glycerol

After each potential hold, 100  $\mu\text{L}$  of electrolyte was sampled, and  $^1\text{H}$  NMR spectra were measured (Figure S3). The conversion of starting glycerol was low due to the large relative volume of the cell compared to the working electrode surface area. Using  $^1\text{H}$  NMR, 1,2-propanediol and formic acid (FA) were determined as the main electrolysis products. The amount of 1,2-propanediol remained constant at different applied potentials, whereas the relative amount of formic acid increased with increasing potential (Table 2). This suggests that the main product of electrolysis at applied potentials was formic acid.

**Table 2.** Relative conversions of starting glycerol at different potential holds after 5 hours. The conversions are calculated based on the integrals of distinct peaks for each compound

WE potential, V vs. RHE	Glycerol conversion, %	Content of formic acid, %	Content of 1,2-propanediol, %
1.35	1.21	0.27	0.94
1.39	1.83	0.83	1.00
1.43	2.41	1.58	0.83
1.49	3.96	2.90	1.06

## Conclusion

In this study, a FeCoNiCu compositionally complex alloy was successfully modified through nitridation (NT) and anodic oxidation (AO), resulting in a highly porous, thin film electrocatalyst with enhanced activity for both the oxygen evolution reaction (OER) and glycerol oxidation reaction (GOR). The synergistic effects of surface treatments yielded a hierarchical structure with significantly increased surface area and optimized active sites, improving catalytic performance. The NT-AO-treated FeCoNiCu catalyst demonstrated good OER activity compared to commercial  $\text{IrO}_x$  benchmarks by achieving lower overpotential requirements in an alkaline electrolyte. The catalyst showcased outstanding performance for glycerol oxidation, effectively lowering the energy input needed for water splitting by substituting OER with GOR. Product analysis during GOR confirmed the formation of formic acid and 1,2-propanediol as key products, highlighting its potential for value-added chemical production. These findings demonstrate that NT-AO surface modification is a powerful strategy for enhancing the electrocatalytic performance of medium entropy alloys and expanding their application in clean energy conversion technologies. Further optimization and testing could unlock the full potential of FeCoNiCu and similar systems for industrial-scale applications in water electrolysis and glycerol valorisation.

**Supplementary material:** Additional data are available electronically on article page of the journal's website: <https://pub.iapchem.org/ojs/index.php/JESE/article/view/2637>, or from the corresponding author upon request.

**Acknowledgments:** The provision of financial support for the research and the preparation of the manuscript by the Slovenian Research Agency (ARIS) within the research programs P2-0393, P2-0118, and I0-0003 and projects MN-0022, N2-0155, J2-3041, N2-0248, and N2-0337 is gratefully acknowledged. Authors further acknowledge funding from the NATO Science for Peace and Security Program (Grant G6230). The authors also thank Edi Kranjc (Department of Inorganic Chemistry and Technology, National Institute of Chemistry, Slovenia) for the X-ray powder-diffraction measurements. The project is co-financed by the Republic of Slovenia, the Ministry of Education, Science and Sport, and the European Union under the European Regional Development Fund.

## References

- [1] X. Du, X. Ma, X. Ding, W. Zhang, Y. He, Enhanced high-temperature oxidation resistance of low-cost Fe-Cr-Ni medium entropy alloy by Ce-adulterated, *Journal of Materials Research and Technology* **16** (2022) 1466-1477. <https://doi.org/10.1016/j.jmrt.2021.12.087>
- [2] D. Wang, L. Liu, M. Chen, H. Zhuang, Electrical and thermal transport properties of medium-entropy SiyGeySnx alloys, *Acta Materialia* **199** (2020) 443-452. <https://doi.org/10.1016/j.actamat.2020.08.053>
- [3] F. Cao, P. Munroe, Z. Zhou, Z. Xie, Medium entropy alloy CoCrNi coatings: Enhancing hardness and damage-tolerance through a nanotwinned structuring, *Surface and Coatings Technology* **335** (2018) 257-264. <https://doi.org/10.1016/j.surfcoat.2017.12.021>
- [4] X. Wang, C. Yang, Y. Zhang, D. Xiong, S. Xu, L. Wang, L. Jiang, P. B. Sorokin, P.K. Chu, Medium-entropy alloy MoCoCu-P as an efficient bifunctional catalyst for water splitting, *Journal of Alloys and Compounds* **988** (2024) 174332. <https://doi.org/10.1016/j.jallcom.2024.174332>
- [5] S. Shuang, G. J. Lyu, D. Chung, X. Z. Wang, X. Gao, H. H. Mao, W. P. Li, Q. F. He, B. S. Guo, X. Y. Zhong, Y. J. Wang, Y. Yang, Unusually high corrosion resistance in MoxCrNiCo medium entropy alloy enhanced by acidity in aqueous solution, *Journal of Materials Science & Technology* **139** (2023) 59-68. <https://doi.org/10.1016/j.jmst.2022.07.061>
- [6] L. Wang, Y. Jiao, R. Liu, D. Wang, Z. Yu, Y. Xi, K. Zhang, S. Xu, H. Liu, L. Wen, X. Xiao, W. Zhang, J. Ji, A Review of Mechanical Properties and Improvement Methods of Medium Entropy Alloys at High Temperature, *Journal of Metals* **76** (2024) 353-361. <https://doi.org/10.1007/s11837-023-06217-3>
- [7] L. Suhadolnik, M. Bele, M. Smiljanić, G. Dražić, L. D. Rafailović, D. Neumüller, M. Šala, A. Logar, N. Hodnik, M. Gaberšček, J. Kovač, U. Trstenjak, T. Montini, M. Melchionna, P. Fornasiero, Enhancing oxygen evolution functionality through anodization and nitridation of compositionally complex alloy, *Materials Today Chemistry* **35** (2024) 101835. <https://doi.org/10.1016/j.mtchem.2023.101835>
- [8] V. Strotkötter, Y. Li, A. Kostka, F. Lourens, T. Löffler, W. Schuhmann, A. Ludwig, Self-formation of compositionally complex surface oxides on high entropy alloys observed by accelerated atom probe tomography: a route to sustainable catalysts, *Material Horizons* **11** (2024) 4932-4941. <https://doi.org/10.1039/d4mh00245h>
- [9] Z. J. Baum, L. L. Diaz, T. Konovalova, Q. A. Zhou, Materials Research Directions Toward a Green Hydrogen Economy: A Review, *ACS Omega* **7** (2022) 32908-32935. <https://doi.org/10.1021/acsomega.2c03996>
- [10] E. A. Moges, K. Lakshmanan, C. Y. Chang, W. S. Liao, F. T. Angerasa, W. B. Dilebo, H. G. Edao, K. T. Tadele, D. D. Alemayehu, B. D. Bejena, C. B. Guta, C. C. Chang, M. C. Tsai, W. N. Su, B. J. Hwang, Materials of Value-Added Electrolysis for Green Hydrogen Production, *ACS*

- Materials Letters Journal* **6** (2024) 4932-4954.  
<https://doi.org/10.1021/acsmaterialslett.4c01173>
- [11] H. H. Dong, Y. X. Zhu, Y. G. Li, J. Y. Liang, Y. Tan, X. Y. Zhang, H. M. Jiang, L. Lin, Z. M. Sun, Recent advances in glycerol valorization through electrocatalytic methods, *Tungsten* **6** (2024) 696-710. <https://doi.org/10.1007/s42864-024-00281-1>
- [12] Q. Wang, J. Li, Y. Li, G. Shao, Z. Jia, B. Shen, Non-noble metal-based amorphous high-entropy oxides as efficient and reliable electrocatalysts for oxygen evolution reaction, *Nano Research* **15** (2022) 8751-8759. <https://doi.org/10.1007/s12274-022-4179-8>
- [13] T. Li, D.A. Harrington, An Overview of Glycerol Electrooxidation Mechanisms on Pt, Pd and Au, *ChemSusChem* **14** (2021) 1472-1495. <https://doi.org/10.1002/CSSC.202002669>
- [14] C. Li, H. Li, B. Zhang, H. Li, Y. Wang, X. Wang, P. Das, Y. Li, X. Wu, Y. Li, Y. Cui, J. Xiao, Z.-S. Wu, Efficient Electrocatalytic Oxidation of Glycerol to Formate Coupled with Nitrate Reduction over Cu-Doped NiCo Alloy Supported on Nickel Foam, *Angewandte Chemie International Edition* **63** (2024) e202411542. <https://doi.org/10.1002/ANIE.202411542>
- [15] L. Fan, B. Liu, X. Liu, N. Senthilkumar, G. Wang, Z. Wen, Recent Progress in Electrocatalytic Glycerol Oxidation, *Energy Technology* **9** (2021) 2000804. <https://doi.org/10.1002/ENTE.202000804>
- [16] Y. Zhou, Y. Shen, J. Xi, X. Luo, Selective Electro-Oxidation of Glycerol into Dihydroxyacetone by PtAg Skeletons., *ACS Applied Materials & Interfaces Journal* **11** (2019) 28953-28959. <https://doi.org/10.1021/ACSAMI.9B09431>
- [17] M. S. E. Houache, K. Hughes, A. Ahmed, R. Safari, H. Liu, G. A. Botton, E. A. Baranova, Electrochemical Valorization of Glycerol on Ni-Rich Bimetallic NiPd Nanoparticles: Insight into Product Selectivity Using in Situ Polarization Modulation Infrared-Reflection Absorption Spectroscopy, *ACS Sustainable Chemistry & Engineering Journal* **7** (2019) 14425-14434. <https://doi.org/10.1021/acssuschemeng.9b01070>
- [18] H. Yao, Y. Wang, Y. Zheng, X. Yu, J. Ge, Y. Zhu, X. Guo, High-entropy selenides: A new platform for highly selective oxidation of glycerol to formate and energy-saving hydrogen evolution in alkali-acid hybrid electrolytic cell, *Nano Research* **16** (2023) 10832-10839. <https://doi.org/10.1007/s12274-023-5842-4>
- [19] L. Fan, Y. Ji, G. Wang, J. Chen, K. Chen, X. Liu, Z. Wen, High Entropy Alloy Electrocatalytic Electrode toward Alkaline Glycerol Valorization Coupling with Acidic Hydrogen Production, *Journal of the American Chemical Society* **144** (2022) 7224-7235. <https://doi.org/10.1021/jacs.1c13740>
- [20] Y. Li, J. Hong, Y. Shen, Application of platinum-based high-entropy-alloy nanoparticles for electro-oxidation of formic acid and glycerol, *International Journal of Hydrogen Energy* **82** (2024) 448-455. <https://doi.org/10.1016/j.ijhydene.2024.07.229>
- [21] L. Suhadolnik, M. Bele, M. Čekada, P. Jovanovič, N. Maselj, A. Lončar, G. Dražić, M. Šala, N. Hodnik, J. Kovač, T. Montini, M. Melchionna, P. Fornasiero, Nanotubular TiOxNy-Supported Ir Single Atoms and Clusters as Thin-Film Electrocatalysts for Oxygen Evolution in Acid Media, *Chemistry of Materials* **35** (2023) 2612-2623. <https://doi.org/10.1021/ACS.CHEMMATER.3C00125>
- [22] W. Zhang, Z. Qu, X. Li, Y. Wang, D. Ma, J. Wu, Comparison of dynamic adsorption/desorption characteristics of toluene on different porous materials, *Journal of Environmental Sciences* **24** (2012) 520-528. [https://doi.org/10.1016/S1001-0742\(11\)60751-1](https://doi.org/10.1016/S1001-0742(11)60751-1)
- [23] R. Luque, A. Ahmad, S. Tariq, M. Mubashir, M. Sufyan Javed, S. Rajendran, R. S. Varma, A. Ali, C. Xia, Functionalized interconnected porous materials for heterogeneous catalysis, energy conversion and storage applications: Recent advances and future perspectives, *Materials Today* **73** (2024) 105-129. <https://doi.org/10.1016/J.MATTOD.2023.05.001>

- [24] X. H. Yan, P. K. Liaw, Y. Zhang, Order and Disorder in Amorphous and High-Entropy Materials, *Metallurgical and Materials Transactions A* **52** (2021) 2111-2122.  
<https://doi.org/10.1007/s11661-021-06250-4>
- [25] K. Kim, T. Kang, M. Kim, J. Kim, Exploring the intrinsic active sites and multi oxygen evolution reaction step via unique hollow structures of nitrogen and sulfur co-doped amorphous cobalt and nickel oxides, *Chemical Engineering Journal* **426** (2021) 130820.  
<https://doi.org/10.1016/J.CEJ.2021.130820>